



Fault Slip Rate of the Kazerun Fault System (KFS), Iran, Investigated Using Finite Element Modeling

BIJAN SHOORCHEH,¹ MAHDI MOTAGH,^{1,2} MARZIEH BAES,² and ABBAS BAHROUDI³

Abstract—A 3D non-homogenous finite element model (FEM) is developed to investigate the spatial variations of interseismic deformation for the Kazerun Fault System (KFS) in the Zagros Mountains of Iran. The model includes 19 fault segments that were extracted from geological maps and previous studies, and the average slips in the dip and strike directions on these segments were computed. The contemporary surface deformation is simulated using a free horizontal detachment surface. The dip angles of the faults in the model are varied at 90°, 70°, 50° and 30° to simulate different 3D representations of the fault systems. Tectonic loading at the boundaries of the region is applied using predicted GPS velocity vectors to the north (southern part of the Central Iran Block) and south (southern region of the Zagros mountain belt), which were obtained by solving inverse and forward problems. Where possible, the fault slip rates that are obtained using our non-homogeneous finite element model are validated using the long-term geologic and instantaneous GPS slip rates. The model is then used to estimate the dip- and strike-slip rates of the fault segments of the KFS for which no a priori information was available. We derive an upper bound of 1 mm/year for the average dip-slip rate in the region, which is consistent with estimates from geomorphologic observations. The modeling results show that in addition to the 4 main faults (Dena, Kazerun, Kareh Bas and Main Recent), other faults, such as the Zagros Front, Main Front, High Zagros and Mishan faults, accommodate up to 2.5 mm/year of the differential movement between the North and Central Zagros. We also investigated the contrast in rigidity between the southern and northern areas of the Zagros mountain belt and found that a rigidity contrast of 2 best explains the GPS data of contemporary surface deformation. Neglecting to account for the rigidity contrast in the model can lead to biased estimates of the fault slip rate of up to 50 %.

Key words: Finite Element, Iran, Zagros, Fault slip rates.

1. Introduction

The Zagros Mountains in Iran are located between the Central Iran Block (CIB) in the north, the Taurus in Turkey to the northwest, the Oman Fault to the southeast and the Persian Gulf to the southwest (FALCON 1967; SCOTT 1981). Active faulting in the area is the result of the collision between the Arabian and Eurasian plates (FALCON 1969).

Geodetic observations from permanent and campaign global positioning system (GPS) networks have been used to investigate the present-day surface velocities and kinematics of the region (TATAR *et al.* 2002; TAVAKOLI *et al.* 2008; VERNANT *et al.* 2004; WALPERSDORF *et al.* 2006). These studies suggest that the current tectonics in the region are characterized by distributed shortening and strike-slip motion along active faults. The strike-slip rates of a limited number of fault segments in the region have been determined in several studies. For example, by measuring the changes in the distances between 14 geodetic benchmarks across the central Zagros Mountains between 1997 and 2000, TATAR *et al.* (2002) suggested that 10 mm/year of shortening is distributed across the mountain belt. VERNANT *et al.* (2004) constrained the right-lateral displacement along the Main Recent Fault (MRF) to be 3 ± 2 mm/year. Walpersdorf *et al.* (2006) showed that the accommodation of convergence between the Arabian and Eurasian plates varies along the Zagros Mountains by deformation partitioning (shortening and dextral strike-slip) and has a maximum of 2 mm/year of strike-slip motion. TAVAKOLI *et al.* (2008) used GPS observations from both campaign and continuous stations to derive strike-slip rates of several fault segments in the region. Using a finite element model

¹ Department of Surveying and Geomatics Engineering, University College of Engineering, University of Tehran, Tehran, Iran. E-mail: b.shoorcheh@ut.ac.ir

² GFZ German Research Centre for Geosciences, 14473 Potsdam, Germany.

³ Department of Mining Engineering, University College of Engineering, University of Tehran, Tehran, Iran.

(FEM), NANKALI *et al.* (2011) investigated the strike-slip rates of several fault segments in the Zagros, including the Main Recent Fault (MRF), the Dena Fault (DF) and the Kazerun Fault (KF).

However, due to the sparsity of geodetic observations and the simple analytical models that have been used for their interpretation, previous studies have focused only on major fault branches that experience strike-slip deformation. Focal mechanism studies from both historical and instrumental earthquakes (BERBERIAN 1995; TALEBIAN and JACKSON 2004; TAVAKOLI *et al.* 2008) indicate that the fault segments in this region have experienced both dip- and strike-slip rupture. Therefore, the detailed roles of all of the geological fault segments in the slip partitioning in the region are not yet well understood.

In this paper, we develop a 3D finite element model to investigate the spatial variations of interseismic deformation in the Kazerun Fault System (KFS) in the Zagros mountain belt of Iran. The KFS subdivides the Zagros mountain belt into the North Zagros and Central Zagros (Fig. 1), which correspond to the northwest part and southeast part of the mountain belt, respectively (BERBERIAN 1995; TALEBIAN and JACKSON 2004). The main geological faults in the region are illustrated in Fig. 1 (BERBERIAN 1995) and include the Main Zagros Reverse Fault (MZRF), Main Recent Fault (MRF), Dena Fault (DF), Kazerun Fault (KF), Borazjan Fault (BF), Kareh Bas Fault (KBF), Sabzpushan Fault (SBZF), Sarvestan Fault (SF), High Zagros Fault (HZF), Main Front Fault (MFF), Zagros Front Fault (ZFF) and Mishan Fault (MF).

Table 1 shows the geologic and geodetic strike-slip rates for several fault segments in the region. In this study, we develop a three-dimensional FEM of the KFS region using planar fault representations to derive the contributions of all of the fault segments in the slip partitioning. This is the first 3D model to incorporate all of the faults in a mechanical model to investigate the active tectonics of the region in terms of the slip rates and locking depths of the faults.

As shown in Fig. 1, the northern and eastern part of the modeling domain is located at the southern margin of the Central Iran Block (CIB), which previous studies suggest is a rigid block within deformation uncertainties of 2 mm/year (NILFORUSHAN *et al.* 2003;

TATAR *et al.* 2002; VERNANT *et al.* 2004; WALPERSDORF *et al.* 2006). The dark gray area in Fig. 2 illustrates this rigid region. Moreover, instrumental seismicity from 2006 to 2009 recorded by the International Institute of Earthquake Engineering and Seismology (<http://www.iiees.ac.ir>) shows that only 20 % of the repeated seismic activity occurs in the northern part of the region (Fig. 2). This seismic observation encourages us to construct a non-homogenous finite element model with different rigidities between the northern and southern Zagros mountain belt. The rigidity contrast (Fig. 2) is investigated by comparing the GPS data and the velocity vectors predicted by the FEM model.

2. Model Setup

One of the main steps in the construction of mechanical models is the geometric representation of the faults. To construct the mechanical model, we began by approximating the geologic fault lines with straight lines in the UTM coordinate system. However, no detailed information about the three-dimensional representation of the faults is available. Previous tectonic studies using focal mechanisms of earthquakes indicate that the faults in the Zagros dip to the NE between 50° and 60° (TATAR *et al.* 2004). We considered 4 scenarios by selecting NE-dipping faults with dip angles of 90°, 70°, 50° and 30° for the FEM model and computed the strike-slip, dip-slip and locking depths for these scenarios.

MARSHALL *et al.* (2009) analytically showed that a semi-infinite vertical strike-slip fault in conventional interseismic deformation models can be replaced by a limited (in vertical depth) fault and a basal horizontal crack (see Appendix A of MARSHALL *et al.* (2009) for the detailed solution). Many studies have used this approach to construct finite element mechanical models and calculate the slip rates and locking status of fault systems (MARSHALL *et al.* 2009, 2013). We build on these studies and extend the faults along their dip angles from the earth's surface to a horizontal freely slipping detachment at a depth of approximately 50 km that represents the Moho (MANAMAN and SHOMALI 2010; PAUL *et al.* 2006). We assume that all of the dip-slip motions are transferred into horizontal motion at the depth of the Moho along

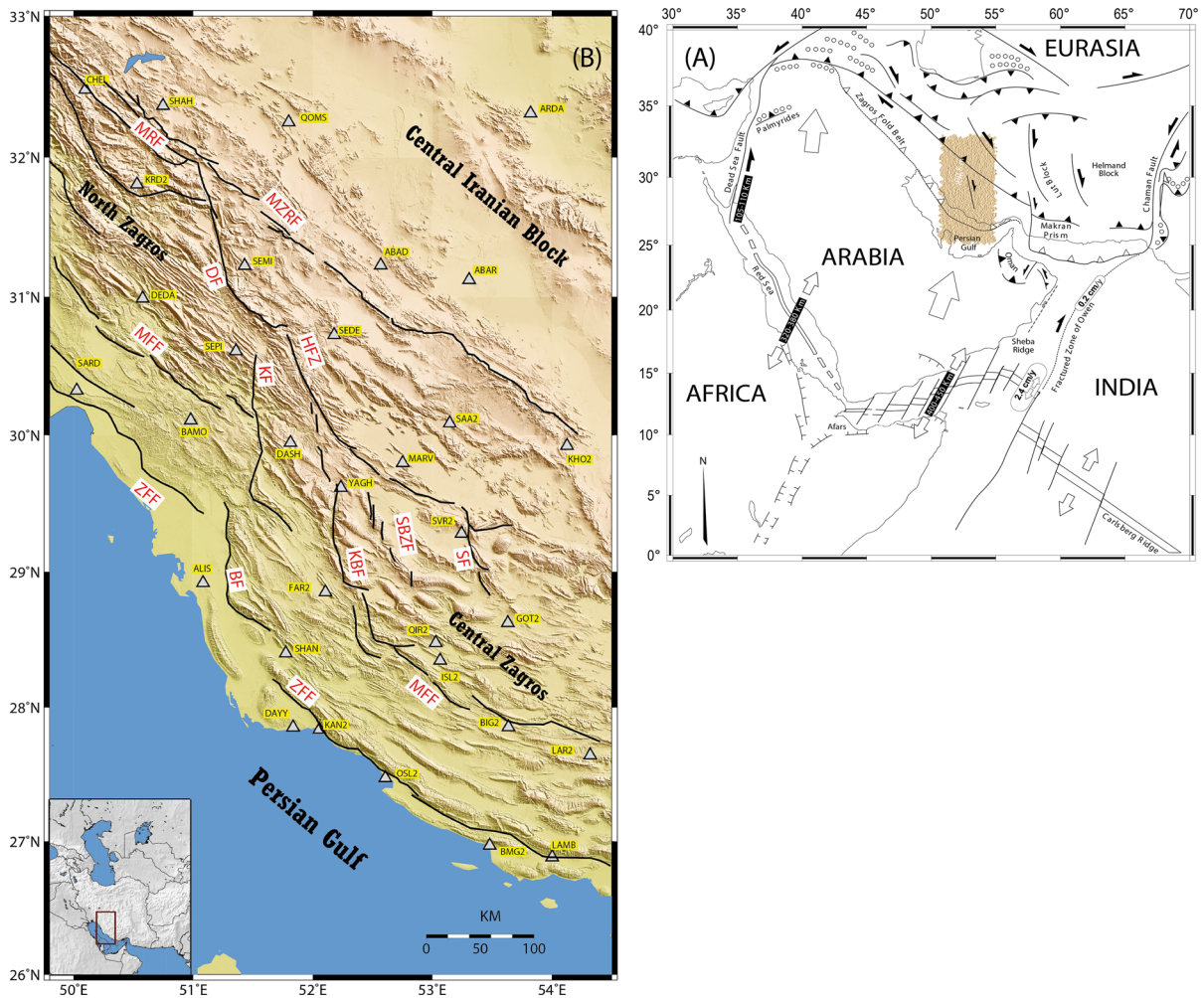


Figure 1

a Map of the Kazerun Fault System relative to the Arabia and Eurasia plates (CARBON 1996). **b** Approximate representations of major active tectonic features (BERBERIAN 1995; AUTHEMAYOU *et al.* 2006). Surface traces of faults are indicated by *black continuous lines*. Geodetic stations from TAVAKOLI *et al.* (2008) and WALPERSDORF *et al.* (2006) are shown by *triangles*. Fault abbreviations are from BERBERIAN (1995) and are as follows. *MZRF* Main Zagros Reverse Fault, *MRF* Main Recent Fault, *MF* Mishan Fault, *DF* Dena Fault, *KF* Kazerun Fault, *BF* Borazjan Fault, *KB* Kareh Bas Fault, *SBZF* Sabzpushan Fault, *SF* Sarvestan Fault, *HZF* High Zagros Fault, *MFF* Main Front Fault, *ZFF* Zagros Front Fault

the modeled stress-free (frictionless) crack. The computational domain has approximate dimensions of $1033 \times 428 \times 50$ km (Fig. 3). Based on the surface projections of the fault segments, we divide the domain along the fault surfaces and construct multiple solid block models for the 3D geometric fault modeling. Adjacent blocks along fault surfaces were constrained to slip along the fault planes, and the other faces of the blocks were tied to adjacent blocks along contact surfaces (Fig. 4). The upper traces of the fault segments were fixed based on geologic

evidence, while the widths of all of the faults varied depending on the dip angle (Fig. 3).

After constructing the solid model that included the faults, we imported all of the blocks into Abaqus, which is a commercial finite element code that is used for numerical modeling (<http://www.simulia.com>). Interseismic, coseismic and postseismic deformation models have been constructed successfully using Abaqus (HUGHES *et al.* 2011; MASTERLARK 2003; MASTERLARK *et al.* 2001, 2010; MASTERLARK and WANG 2002). Because the faults are planar, the FEM

Table 1
Geologic and geodetic strike-slip rate

Full description fault name	Raw description fault name	Slip sense	Average geological slip rate		GPS derived slip rate (TAVAKOLI <i>et al.</i> 2008)		GPS derived slip rate (WALPERSDORF <i>et al.</i> 2006)	
			Low rate limit (mm/year)	High rate limit (mm/year)	Low rate limit (mm/year)	High rate limit (mm/year)	Low rate limit (mm/year)	High rate limit (mm/year)
Dena	DF	Right-lateral	3	5	2.9	4.5	1	5
Kazerun	KF	Right-lateral	1	3	3	4.2	–	–
Borazjan	BF	Right-lateral	–	–	0	1	–	–
Kareh Bas	KBF	Right-lateral	–	–	3.1	3.7	0	4
Main Recent	MRF	Right-lateral	6	10	–	–	0.5	4.5

Geologic slip rates are from AUTHEMAYOU *et al.* (2006). GPS slip rates are from WALPERSDORF *et al.* (2006) and TAVAKOLI *et al.* (2008)

models were constructed using linear tetrahedral elements with an element size of 5 km along the fault surfaces. We utilized linear elastic and isotropic constitutive models in the FEM model.

Data from campaign-mode GPS stations, the Iranian Permanent GPS Network (IPGN) and the International GNSS Service (IGS) were measured and analyzed using the GAMIT/GLOBK 10.1 software by WALPERSDORF *et al.* (2006) and TAVAKOLI *et al.* (2008), and GPS velocities were estimated relative to the ITRF2000 reference frame (ALTAMIMI *et al.* 2002). These velocity fields were used to establish the tectonic loading boundary conditions. Because the GPS velocity field from TAVAKOLI *et al.* (2008) was designed specifically for the KFS and covers the region well, we mainly used GPS data from that study to load our model, except for stations BMG2 and LAMB, which are located in the southeast part of the region and for which we used the results from WALPERSDORF *et al.* (2006).

The boundary conditions are determined based on estimates of the average regional strain rate along with a regional rate of vertical axis rotation (COOKE and MARSHALL 2006; GRIFFITH and COOKE 2005; MARSHALL *et al.* 2008, 2009, 2013). Two steps were used to implement this in the FEM using GPS velocity vectors. First, we used the horizontal velocities in ITRF2000 and solved a least-squares inverse problem to obtain six parameters, including two

translation and four velocity gradient tensors (ALLMENDINGER *et al.* 2007). The inversion results in a best-fitting principle contraction rate of 22 nanostains/year that is oriented at N25.9°E, a principle extension rate of 5 nanostrains/year oriented perpendicular to the contraction direction, and a regional vertical axis rotation rate of 0.2°/Myr. Our estimates of the principle strain rates and their directions are consistent with a recent study (ZARIFI *et al.* 2013). Second, using the six estimated parameters and by solving a forward problem, we estimated the velocities of the nodes on the four sides (west, east, north and south) of the finite element model and loaded the model using these velocities. The bottom boundary condition of the model was defined by a frictionless horizontal crack at the base of the model. Figure 5 shows the estimated velocity vectors that were used to simulate the regional tectonic boundary loading.

To investigate the locking depth, we assume that the locking depths of all of the segments of the KFS fault system are the same and varied them all from 0 to 20 km at 5 km intervals. To implement the locking depth in the FEM models, we followed the two-step procedure of MARSHALL *et al.* (2009, 2013) that is based on the classic back-slip concept (SAVAGE 1983). First, we apply the boundary conditions that were derived from the method described above to a model with a zero locking depth (the so-called geological

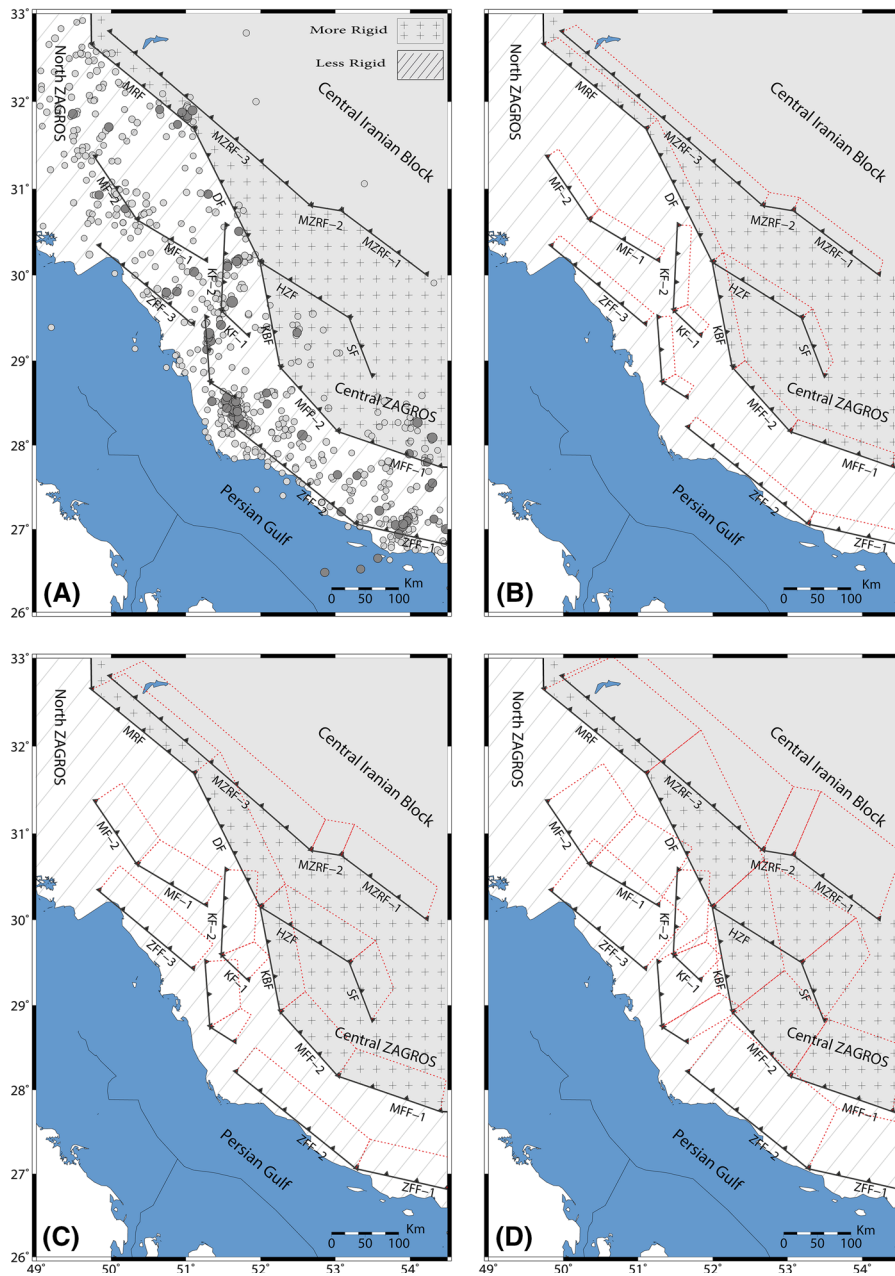


Figure 2

Representations for models with dips of 90° (a), 70° (b), 50° (c) and 30° (d). A total of 19 fault segments were fitted to the Kazerun fault system. The continuous black lines in a–d represent the upper and lower fault tips. A horizontal crack represents the average Moho surface in the region at a depth of 50 km. In a, the width of all of the vertical fault segments is the same as the Moho depth. The light and dark gray circles in a show $3.5 < M_w < 4.5$ and $M_w > 4.5$ earthquakes from 2006 to 2013, respectively. The fault names are the same as in Fig. 1 and are followed by numbers that indicate fault segments. The gray region with the plus sign shows the area of higher rigidity

time-scale model) and extract the slips at the nodes on the basal crack at the bottom of the model and on the left and right sides of the faults. Second, all of the blocks from the ground to the locking depth are cut

and merged together based on their rigidity values to derive northern and southern blocks that correspond to the proposed contrast in rigidity. We then tie the bottoms of these 2 blocks to the tops of the other

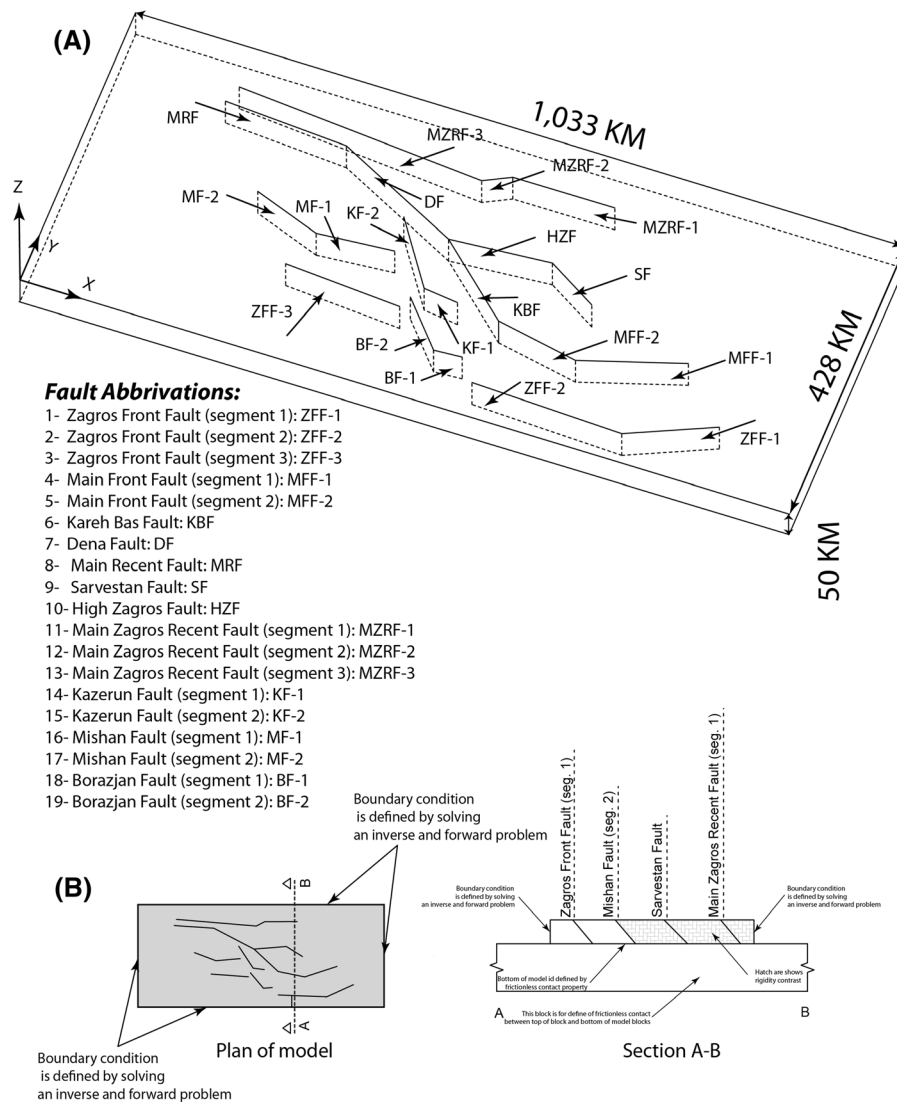


Figure 3

a Fault system geometry including 19 segments that extend vertically (dip angle of 90°) to the free horizontal detachment at the depth of the Moho. **b** Plan view and cross section of the model

blocks below the locking depth to define the locking depth. Due to the reconfiguration of the blocks, the blocks must be remeshed, which creates new nodes on the left and right sides of the fault planes and on the bottom of the model. To implement the back-slip approach, we extract the node coordinates at the bottom of the model and along the left and right sides of the faults below the locking depth and then compute their slip values using the slip on the nodes in the geological time-scale model. After loading the FEM model, we can compare the surface velocities that are

predicted from the model with those observed by GPS.

3. Results

3.1. Rigidity Contrast and Locking Depth

The key parameters in elastic models of interseismic deformation are the fault locking depth and the slip rate (BARBA *et al.* 2013; CARAFA and BARBA 2011;

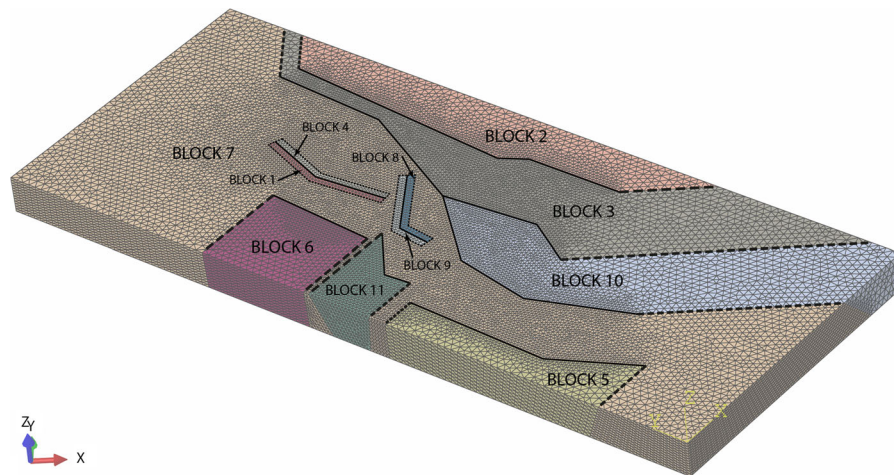


Figure 4

Different blocks of our FEM model. The model was subdivided into 11 distinct blocks. The continuous and dashed lines show the limits of the blocks. After meshing, the blocks were constrained to slip along the fault surfaces (*continuous lines*), and in other areas the blocks are connected (*dashed lines*)

HSU *et al.* 2011; MASTERLARK *et al.* 2001). As explained previously, seismic observations show that more seismic activity is present in the southern part of Zagros than in the north (Fig. 2a). To investigate the rigidity contrast between these two blocks, we constructed several scenarios with rigidity contrasts ranging from 1 to 5. The material properties adapted for the blocks are summarized in Table 2.

A trial-and-error approach was used to determine the lateral heterogeneities (stiffness contrast between the northern and southern parts) and locking depth that minimize the Root Mean Square (RMS) error between the measured GPS velocities and those predicted by the model for the 4 scenarios with dip angles of 90° , 70° , 50° and 30° . Figure 6 shows a plot of the rigidity contrast versus the RMS. As shown in Fig. 6a–d, for fault systems with dip angles of 90° , 70° and 50° , the minimum RMS occurs with a rigidity contrast of 2 and a locking depth of 5 km. For the fault system with a dip angle of 30° , the minimum RMS occurs with a rigidity contrast of 1 and a locking depth of 0 km. Figure 6E shows the variation of RMS versus rigidity contrast for a locking depth of 5 km. Figure 6F shows the variation in RMS versus locking depth for a rigidity of 2. A rigidity contrast of 2 gives the minimum RMS for these dip angles. Figure 6F shows that increase in the locking depth from 0 to 5 km decreases the RMS error. However, changes in the locking depth between 5 and 20 km do

not significantly change the RMS error ($<2\%$). This is because the GPS stations that were used in this study were originally designed to sense off-fault velocity and to accurately measure the strain induced from the locking depth, so they are not near the faults (TAVAKOLI *et al.* 2008). Figure 7 shows the residuals between the GPS observations and the model velocities for fault systems with dip angles of 90° , 70° and 50° (rigidity contrast of 2 and locking depth of 5 km) as well as for the fault system with a dip angle of 30° (rigidity contrast of 1 and locking depth of 0 km). The variation of dip angle does not significantly change the residuals at the GPS stations.

Because the present distribution of GPS stations in this region can only help us investigate the long-term slip rate, in the following computation we constrained the rigidity contrast between the northern and southern parts of our models for the 4 scenarios (rigidity contrast of 2 with dips of 90° , 70° , 50° and a rigidity contrast of 1 for a dip of 30°) and determine the slip rates along the active geologic structures in the region. We also assess the effect of non-homogeneity of the medium on the fault slip rates.

3.2. Slip Rate Determination and Model Validation

To determine the slip rates of the fault segments in the model, we initially derive the velocities for all of the nodes of the model and then search the nodes

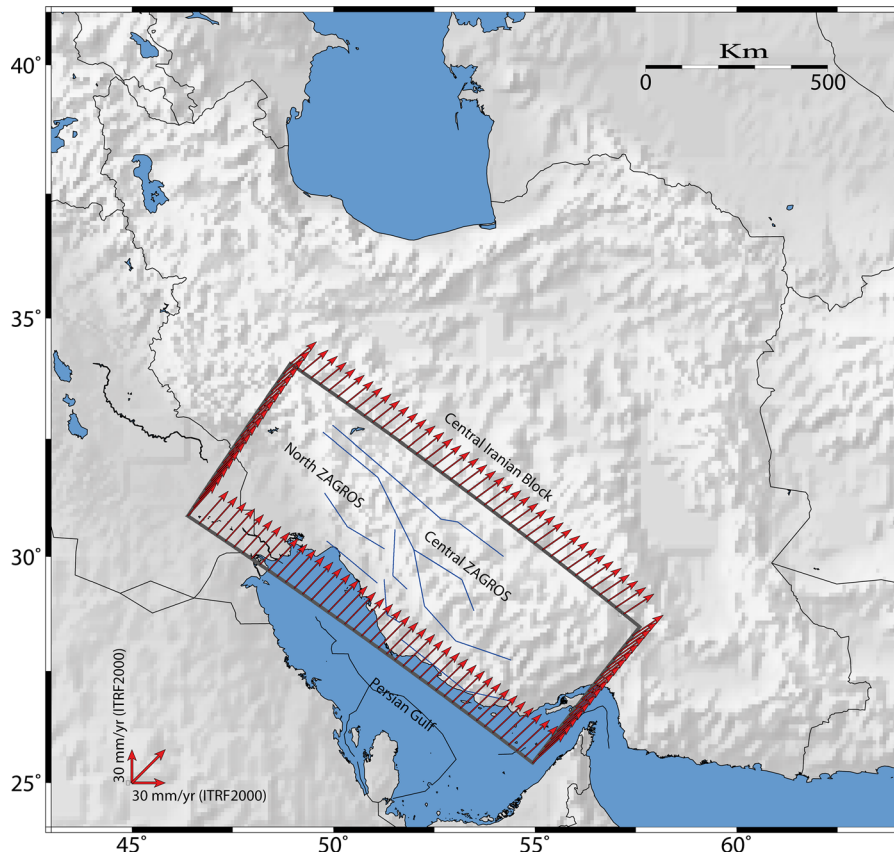


Figure 5

Plan view of the study area with fault segments marked as blue lines. The velocity vectors that were used as boundary conditions along the edges of the model were obtained by solving an inverse problem using the GPS velocity observations reported by WALPERSDORF *et al.* (2006) and TAVAKOLI *et al.* (2008) and then solving a forward problem on the nodes along the northern, eastern, southern and western boundaries of the model

Table 2

Material properties selected for 11 blocks of region to investigate rigidity contrast of north and south of region

Model number	Young's modulus for blocks 1, 4, 5, 6, 7, 8,9 and 11 (Pa)	Young's modulus for blocks 2, 3 and 10 (Pa)	Poisson's ratio
1	1e11	1e11	0.25
2	1e11	2e11	0.25
3	1e11	3e11	0.25
4	1e11	4e11	0.25
5	1e11	5e11	0.25

Values of model 1 adapted from VERNANT and CHÉRY (2006)

that are located on the left and right blocks along the fault planes. Because the node velocities are relative to ITRF2000, we transform the velocities and node coordinates from ITRF2000 to a local coordinate system, which is defined by the origin on the lower-left side of the fault, X and Y axes along the fault

surface and the Z axis perpendicular to the fault surface. The velocities for the left and right nodes on the fault plane are then subtracted from each other to compute the values of the strike- and dip-slip. Because we have variable slip vectors at the element nodes along the fault surfaces, we use all of the fault

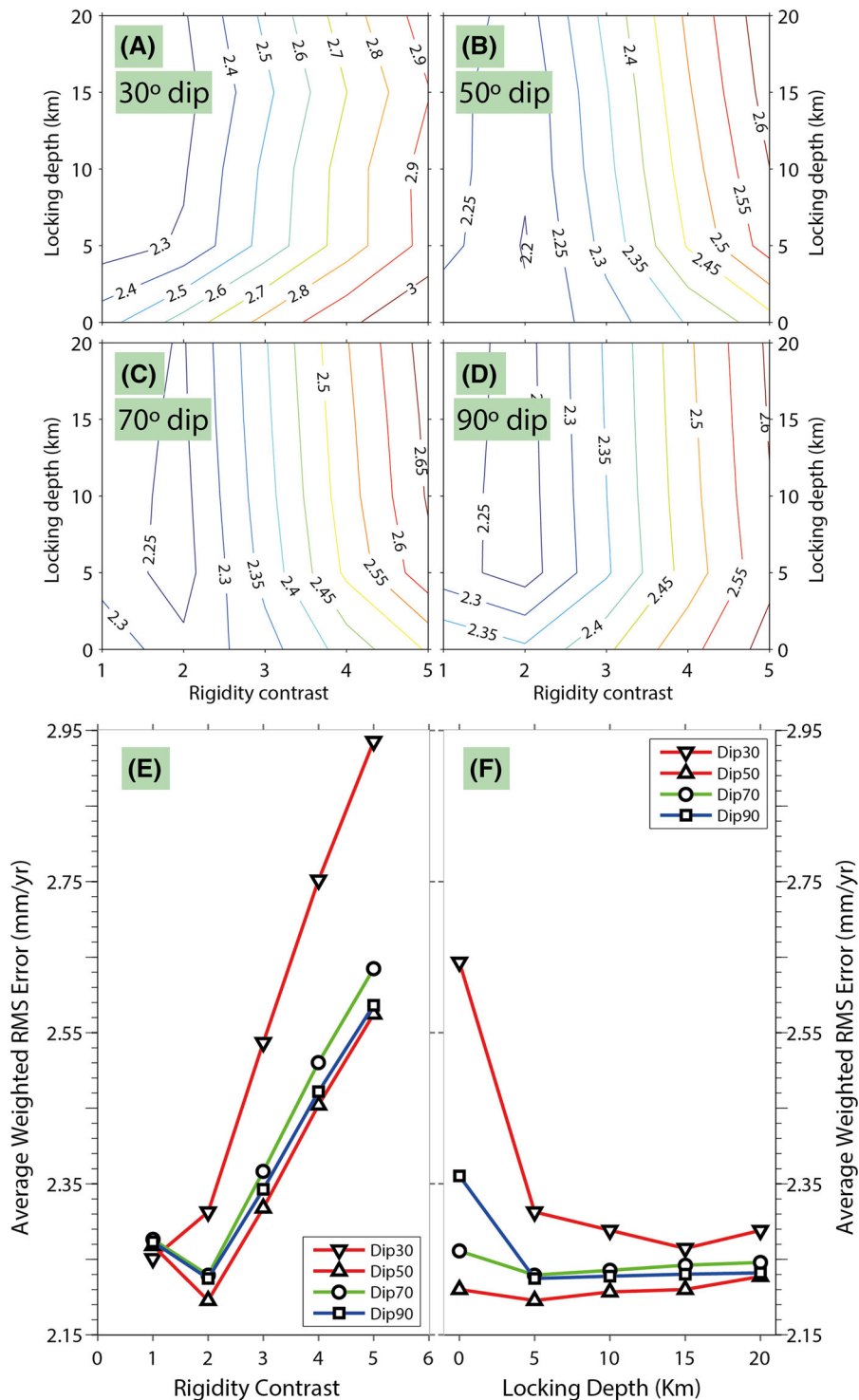


Figure 6

a–d Show variations of the average residual RMS errors versus locking depth and rigidity contrast for models with fault dip angles of 30°, 50°, 70° and 90°. The minimums for models **b–d** occur for a locking depth of 5 km and a rigidity contrast of 2. The minimum for model **a** occurs for a locking depth of 0 km and a rigidity contrast of 1. **e, f** Show the variations of RMS for a locking depth of 5 km and a rigidity contrast of 2, respectively. Locking depths of 5–20 km do not significantly change the RMS

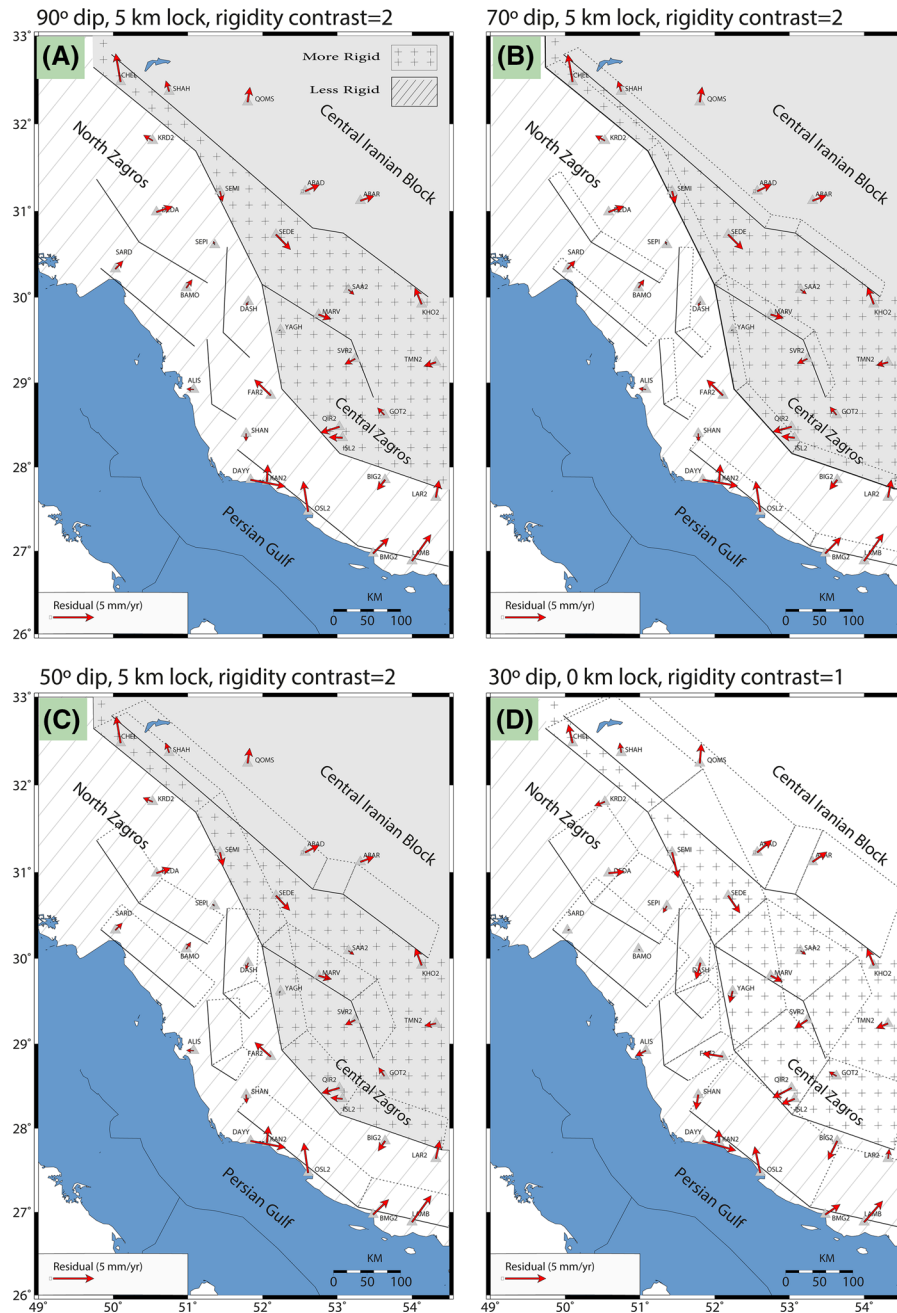


Figure 7

a–c Show the residuals for models with a locking depth of 5 km and a rigidity contrast of 2. **d** Corresponds to the model with a locking depth of 0 km and a rigidity contrast of 1. The dark area shows the region of higher stiffness

elements and compute a weighted average of the slip vectors at the element nodes based on the area of the elements to extract the slip rates.

For each dip angle, we ran 20 models by varying the rigidity contrast from 1 to 5 and the locking depth

from 0 to 20 km at 5 km intervals to compute the slip in the strike and dip directions (Figs. 8, 9, 10). We then compared the results to available geologic and geodetic slip rates. Of the 19 fault segments that were studied, the strike-slip rates for only 5 segments have

been constrained by previous studies, including the Dena, Main Recent, Kazerun (seg. 2), Kareh Bas and Borazjan (seg. 2) faults (AUTHEMAYOU *et al.* 2009; TAVAKOLI *et al.* 2008; WALPERSDORF *et al.* 2006). As shown in Fig. 8, the results of our model for these 5 segments agree well with those of the previous studies. Moreover, if we assume two likely models with dip angle of 50° and 60° for the fault segments based on TATAR *et al.* (2004), the average dip-slip rates for 19 segments corresponding to dip angle of 50° and 60° are 0.7 and 0.9 mm/year (Table 3), respectively, and the upper bound for the average dip-slip rate of 19 fault segments in the region is <1 mm/year, which is consistent with estimates from geomorphologic observations (FALCON 1974). We take these two outcomes as a validation of our model and estimate the strike- and dip-slip rates for the other fault segments in the region.

Table 3 lists the strike- and dip-slip components for all of the fault segments using an average dip angle of 50°–60° and a rigidity contrast of 2, and Table 4 shows the effect of the change in dip angle (from 30°–90°) and rigidity contrast (from 1 to 5) on the amount of strike- and dip-slip. To better evaluate these effects, we subdivide the faults into three groups, including faults that are located (1) in the southern part of the region with lower rigidity, (2) along the boundary between the northern and southern parts, and (3) in the northern part with higher rigidity. For all 19 fault segments, we plot the net, strike- and dip-slip rates (Figs. 11, 12, 13) and compute the lower and upper limits of variation (Table 4). By decreasing the dip angle from 90° to 30°, the fault width and area increase. Thus, models with a dip angle of 90° have the minimum area, and models with a dip angle of 30° have the maximum

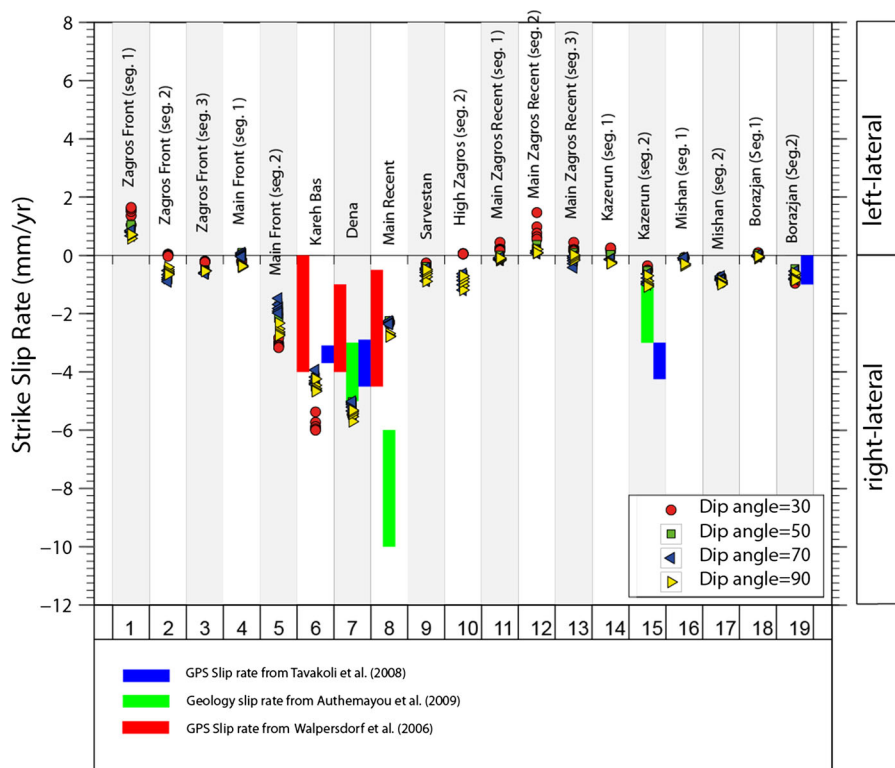


Figure 8

Strike-slip rates for 19 fault segments within the KFS from the forward mechanical models. Yellow triangles, blue triangles, squares and circles show strike-slip rates for faults with dip angles of 90°, 70°, 50° and 30°, respectively, from models with rigidity contrasts of 1–5. The ranges of geologic slip rates from AUTHEMAYOU *et al.* (2009) are shown by green rectangles, and GPS slip rates estimated by TAVAKOLI *et al.* (2008) and WALPERSDORF *et al.* (2006) are shown with blue and red rectangles, respectively

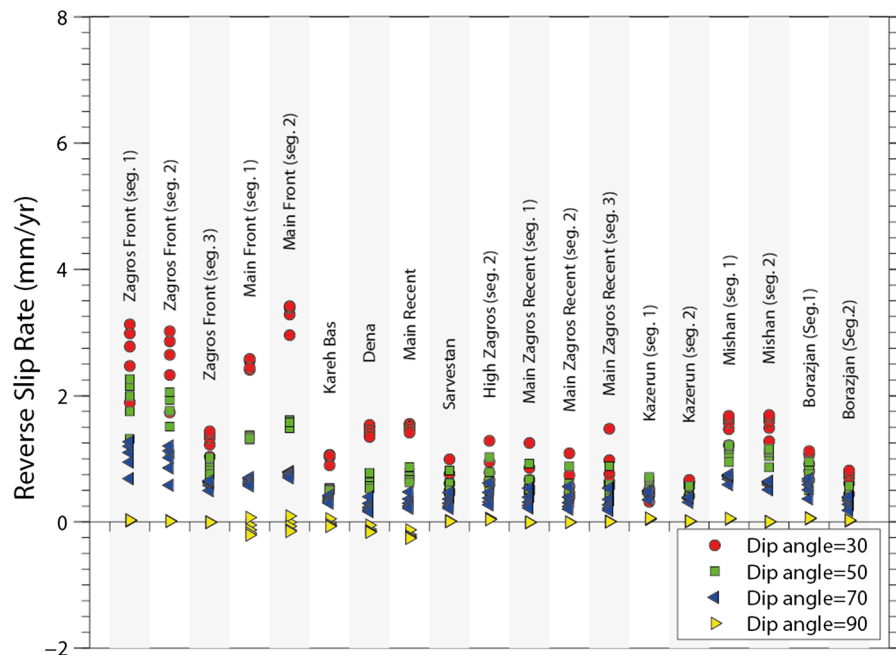


Figure 9

Dip-slip rates for 19 fault segments within the KFS from forward mechanical models. *Triangles, squares and circles* show strike-slip rates for faults with different dip angles

area. Figure 11 shows that models with higher fault areas generally have higher net slip rates. The net slips for all 19 segments are incremental except for segments 5–8, which show that the net slip for a 90° dip angle is greater than those for 70° and 50° dip angles and is less than that for a 30° dip angle. By increasing the rigidity contrast from 1 to 5, the net slip of the segments in group 1 will increase, while the net slip rate of those in group 3 will decrease. In group 2, the slip rates on segments 5 and 6 increase, the rate on segment 7 decreases, and the rates for segments 4 and 8 show irregular behavior. As shown in Fig. 12, the reverse slip rates for all 19 segments are close to zero for a dip angle of 90° . The reverse slip increases when the dip angle decreases. By increasing the rigidity contrast from 1 to 5, the reverse slip rates of the segments in group 1 increase, while the reverse slip rates of the segments in group 3 decrease. For the faults in group 2, the slip rates on segments 7 and 8 decrease, while segments 4, 5 and 6 show irregular behaviors. We do not observe increases and decreases of strike-slip similar to those that are observed for the net and dip-slip. An interesting point about the variation of the strike-slip rate is that the

slip sense (left or right lateral) of several segments (10, 11, 13, 14 and 18) changes from right lateral to left lateral (Fig. 13). As shown in Table 4, the sensitivity of the dip-slip to the dip angle is greater than the sensitivity of the strike-slip. The maximum variations of the strike-and dip-slip motions occur on the Kareh Bas (5 ± 1 mm/year) and Main Front (seg. 2) (1.6 ± 1.8 mm/year) faults. Of the 19 segments, the strike-slip components of only 5 segments vary by more than 1 mm/year, while the dip-slip components of 16 segments vary by more than 1 mm/year.

For the dip angle of 50° – 60° , a comparison of the slip rates estimated with a rigidity contrast of 2 with those estimated with rigidity contrasts of 1 (Table 5) shows that the net slip rate changes by up to 50 %.

4. Discussion

Three-dimensional representations of the fault system with the fault tips at the ground surface were constructed to study the detailed kinematics of fault deformation in the Kazerun Fault System (KFS) in the Zagros Mountains of Iran. The FEM modeling

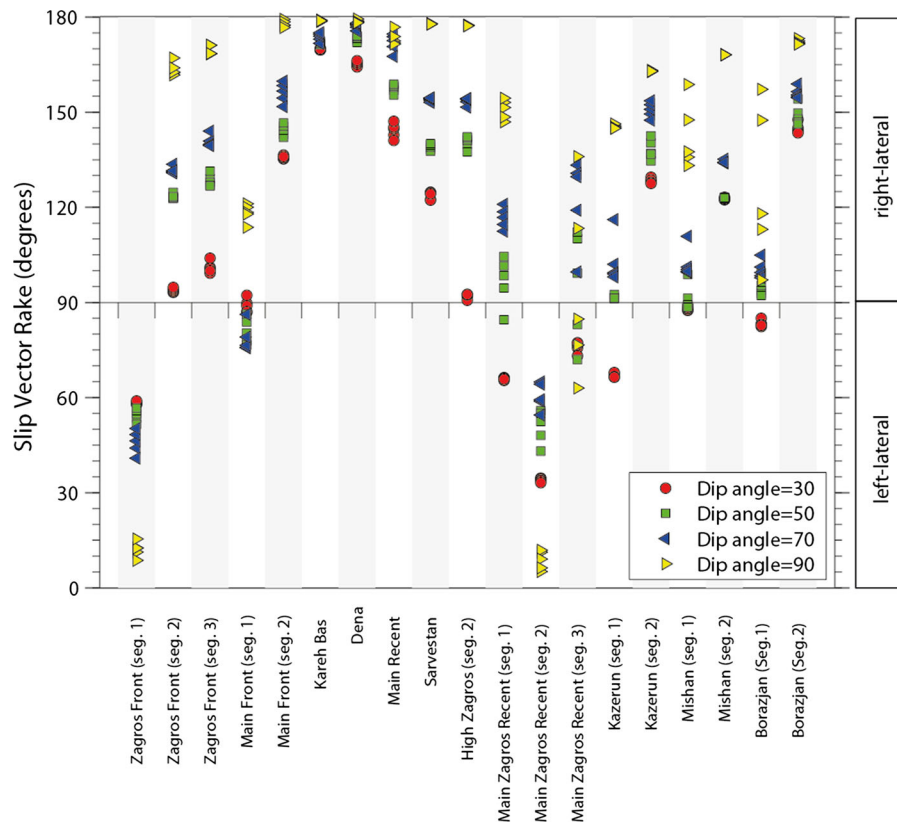


Figure 10

Rake angles of fault segments estimated from the strike- and dip-slip components. A slip vector of 90° indicates pure reverse slip, and slip vectors of 0 and 180° indicate pure left-lateral and pure right-lateral strike-slip, respectively. *Yellow triangles, blue triangles, squares and circles* represent rake angles for faults of the KFS with dip angles of 90° , 70° , 50° and 30° , respectively

provided insight into the rheology and detailed role of the geological fault segments in the slip partitioning in the region.

In other studies, elastic, visco-elastic and visco-elasto-plastic rheologies have been used to model interseismic deformation (BARBA *et al.* 2013; MARSHALL *et al.* 2009, 2013; SAVAGE 1983; SAVAGE and PRESCOTT 1978). Previous studies suggest that the average viscosity below the Zagros Mountains is $>10^{22}$ Pa s (NANKALI 2011). Because of this high viscosity, we consider a linear elastic rheology to be an appropriate model to describe interseismic surface deformation in the KFS.

As shown above, we obtained a higher rigidity for the northern and eastern blocks (blocks 2, 3 and 10) than the southern and western blocks (blocks 1, 4, 5, 6, 7, 8, 9 and 11). Ignoring this variation in the elastic parameters affects our estimates of the slip rates by 50 %.

This change in rigidity is consistent with the pattern of seismicity in the study region, which contains more seismicity in the south than in the more rigid northern region. However, it should be noted that the presence of a rigidity contrast does not necessarily require a difference in the pattern of seismicity. For example, the Ventura Basin in southern California has a much lower stiffness than the more rigid mountains (HAGER *et al.* 1999), but there are few earthquakes in the Ventura basin compared to other regions of southern California.

Based on an analysis of seismicity depth, TATAR *et al.* (2004) proposed a seismogenic layer at depths of 8–15 km in the central Zagros. However, recent studies have shown that the seismicity can occur at shallower depths of 1–5 km (LOHMAN and SIMONS 2005), which is consistent with the lower bound of 5 km for the locking depth that we obtained in this region. Because of the sparse distribution of the GPS

Table 3
Along-strike, along-dip and total slip rates along modeled fault surfaces for dip angle of 60°–50°

No.	Fault	Strike (mm/year)		Dip				Net (mm/year)	
		Dip 60°	Dip 50°	Dip 60°		Dip 50°		Dip 60°	Dip 50°
				Heave (mm/year)	Throw (mm/year)	Heave (mm/year)	Throw (mm/year)		
1	Zagros Front (seg. 1)	0.87	0.95	0.68	1.17	1.13	1.34	1.10	1.65
2	Zagros Front (seg. 2)	−0.64	−0.61	0.59	1.02	0.97	1.16	0.87	1.31
3	Zagros Front (seg. 3)	−0.55	−0.49	0.37	0.63	0.57	0.68	0.66	0.84
4	Main Front (seg. 1)	0.07	0.08	0.51	0.89	0.88	1.05	0.52	1.05
5	Main Front (seg. 2)	−1.80	−1.91	0.60	1.04	1.03	1.23	1.90	2.27
6	Kareh Bas	−4.28	−4.38	0.23	0.40	0.35	0.41	4.29	4.40
7	Dena	−5.27	−5.32	0.24	0.42	0.44	0.52	5.27	5.35
8	Main Recent	−2.30	−2.29	0.29	0.50	0.50	0.60	2.32	2.37
9	Sarvestan	−0.65	−0.59	0.24	0.42	0.39	0.47	0.69	0.76
10	High Zagros	−0.96	−0.91	0.31	0.55	0.51	0.61	1.01	1.10
11	Main Zagros Recent (seg. 1)	−0.13	−0.09	0.26	0.46	0.43	0.51	0.29	0.52
12	Main Zagros Recent (seg. 2)	0.17	0.26	0.25	0.43	0.39	0.47	0.30	0.53
13	Main Zagros Recent (seg. 3)	−0.20	−0.11	0.24	0.41	0.38	0.45	0.31	0.46
14	Kazerun (seg. 1)	−0.06	0.01	0.26	0.44	0.37	0.45	0.26	0.45
15	Kazerun (seg. 2)	−0.72	−0.65	0.22	0.38	0.32	0.38	0.75	0.76
16	Mishan (seg. 1)	−0.11	−0.11	0.44	0.76	0.70	0.83	0.45	0.84
17	Mishan (seg. 2)	−0.80	−0.82	0.41	0.71	0.67	0.80	0.89	1.14
18	Borazjan (seg. 1)	0.00	0.01	0.30	0.52	0.45	0.53	0.30	0.53
19	Borazjan (seg. 2)	−0.63	−0.58	0.17	0.29	0.25	0.30	0.65	0.65

Negative strike-slip rates refer to right-lateral and positive refer to left-lateral. All dip-slip rates are positive and refer to reverse slip

velocities, our modeling cannot accurately constrain the locking depth below 5 km. Denser GPS observations will help to better constrain the locking depth for individual fault segments in the KFS (AMORUSO *et al.* 2013).

Considering average dip angles of 50° and 60° (Table 3), the average model-predicted strike-slip rate for the Dena Fault is 5.3 mm/year, which is similar to the upper rate predicted by geologic and geodetic observations (see Table 2). The modeled strike-slip rate of 2.3 mm/year for the Main Recent Fault is slower than the geological estimate of (6–10 mm/year) but is within the range of geodetic slip rates of 0.5–4.5 mm/year. The modeled strike-slip rate for the Kazerun Fault of 0.7 mm/year is similar to the lower bound of geologic slip rates (1–3 mm/year) but is lower than the geodetic slip rate (3–4.2 mm/year). For the Borazjan Fault (seg. 2), the modeled strike-slip rate of 0.6 mm/year is within the

geodetic slip range (0–1 mm/year). The modeled strike-slip rate of 4.3 mm/year for the Kareh Bas Fault is similar to the upper limits of the geodetic slip rates (3.1–3.7 and 0–4 mm/year). Despite the small discrepancies, there is a good correlation between the modeled slip rates and the geologic and geodetic strike-slip rates. The reverse slip rates for the Dena and Main Recent faults (Fig. 9) are slower than the strike-slip rates, and the net slips of these three faults are affected mainly by their strike-slip rates. The good match between the geologic and GPS slip rates with the results of our models for the main branches of the KFS validates the mechanical models that we developed to determine the strike- and dip-slip rates for other unconstrained faults in this region for which no a priori information is available.

All of the computed dip-slip rates from our model show reverse slip, which is consistent with the compressional tectonic regime of the KFS (JACKSON and

Table 4

Lower and upper limit of along-strike, along-dip and total slip rates along modeled fault surfaces due to variation of dip angle and rigidity contrast of fault systems

No.	Fault	Strike (mm/year)		Dip (mm/year)		Net (mm/year)	
		Lower limit	Upper limit	Lower limit	Upper limit	Lower limit	Upper limit
1	Zagros Front (seg. 1)	0.6	1.6	0.0	3.1	0.6	3.5
2	Zagros Front (seg. 2)	-0.9	0.0	0.0	3.0	0.9	3.0
3	Zagros Front (seg. 3)	-0.6	-0.2	0.0	1.4	0.6	1.4
4	Main Front (seg. 1)	-0.4	0.1	-0.2	2.6	0.5	2.6
5	Main Front (seg. 2)	-3.2	-1.5	-0.2	3.4	3.2	3.7
6	Kareh Bas	-6.0	-3.9	-0.1	1.1	4.1	6.0
7	Dena	-5.7	-5.0	-0.2	1.5	5.2	5.7
8	Main Recent	-2.8	-2.2	-0.3	1.6	2.7	2.8
9	Sarvestan	-0.9	-0.3	0.0	1.0	0.9	1.0
10	High Zagros	-1.2	0.1	0.0	1.3	1.2	1.3
11	Main Zagros Recent (seg. 1)	-0.2	0.4	0.0	1.3	0.2	1.3
12	Main Zagros Recent (seg. 2)	0.1	1.5	0.0	1.1	0.1	1.8
13	Main Zagros Recent (seg. 3)	-0.4	0.5	0.0	1.5	0.4	1.5
14	Kazerun (seg. 1)	-0.3	0.3	0.0	0.7	0.3	0.8
15	Kazerun (seg. 2)	-1.1	-0.4	0.0	0.7	0.8	1.1
16	Mishan (seg. 1)	-0.4	-0.1	0.0	1.7	0.4	1.7
17	Mishan (seg. 2)	-1.0	-0.7	0.0	1.7	1.0	1.8
18	Borazjan (seg. 1)	-0.1	0.1	0.0	1.1	0.1	1.1
19	Borazjan (seg. 2)	-1.0	-0.5	0.0	0.8	0.9	1.0

FITCH 1981; MAGGI *et al.* 2000; NI and BARAZANGI 1986). Previous studies have shown that the fault segments of the KFS show right-lateral slip (BERBERIAN 1995; TALEBIAN and JACKSON 2004). Regardless of the dip angle selected for the modeling, we derive right-lateral motion for the majority of the fault segments in the KFS (Fig. 10), which is consistent with the tectonic regime derived from the inversion of focal mechanisms (ZARIFI *et al.* 2013). The only exception is for the Zagros Front (seg.1), Main Front (seg. 1) and Main Zagros Recent (seg. 2) faults, which show left-lateral motion that is not favored by the regional tectonic regime. The left-lateral motion results from the GPS velocities at stations BMG2 and LAMB, which show little obliquity between the velocity vectors in the southeast part of the GPS network and the true convergence direction of at least N13°E in this area. Future GPS observations at this part of the network are necessary to resolve this issue and better constrain the amount and sense of slip on the Zagros Front (seg.1), Main Front (seg. 1) and Main Zagros Recent (seg. 2) faults.

Several previous studies have attempted to provide information and constraints on the kinematics of the Zagros from GPS observations. TATAR *et al.* (2002) estimated 10 mm/year of shortening for the central Zagros, and NILFOROUSHANET *et al.* (2003) obtained 6 and 3 mm/year of shortening for the Central and Northern Zagros, respectively. VERNANT *et al.* (2004) attributed 8 mm/year of shortening to the Central Zagros. WALPERSDORF *et al.* (2006) attributed 3–6 and 6–10 mm/year of shortening to the northwest and southeast Zagros, respectively, and a total of 4–6 mm/year of dextral strike-slip motion to the region northwest of the Zagros with no individual strike-slip faults with slips of more than ~2mm/year. TAVAKOLI *et al.* (2008) quantified the slip rates of the Dena, Kazerun and Kareh Bas faults and examined their consistency with geological slip rates. These studies provide an important overview of the large-scale tectonic regime of the Zagros, but none of them used numerical modeling to interpret the results in detail. Using the FEM, we are able to derive off-fault motions for all active segments in the region that

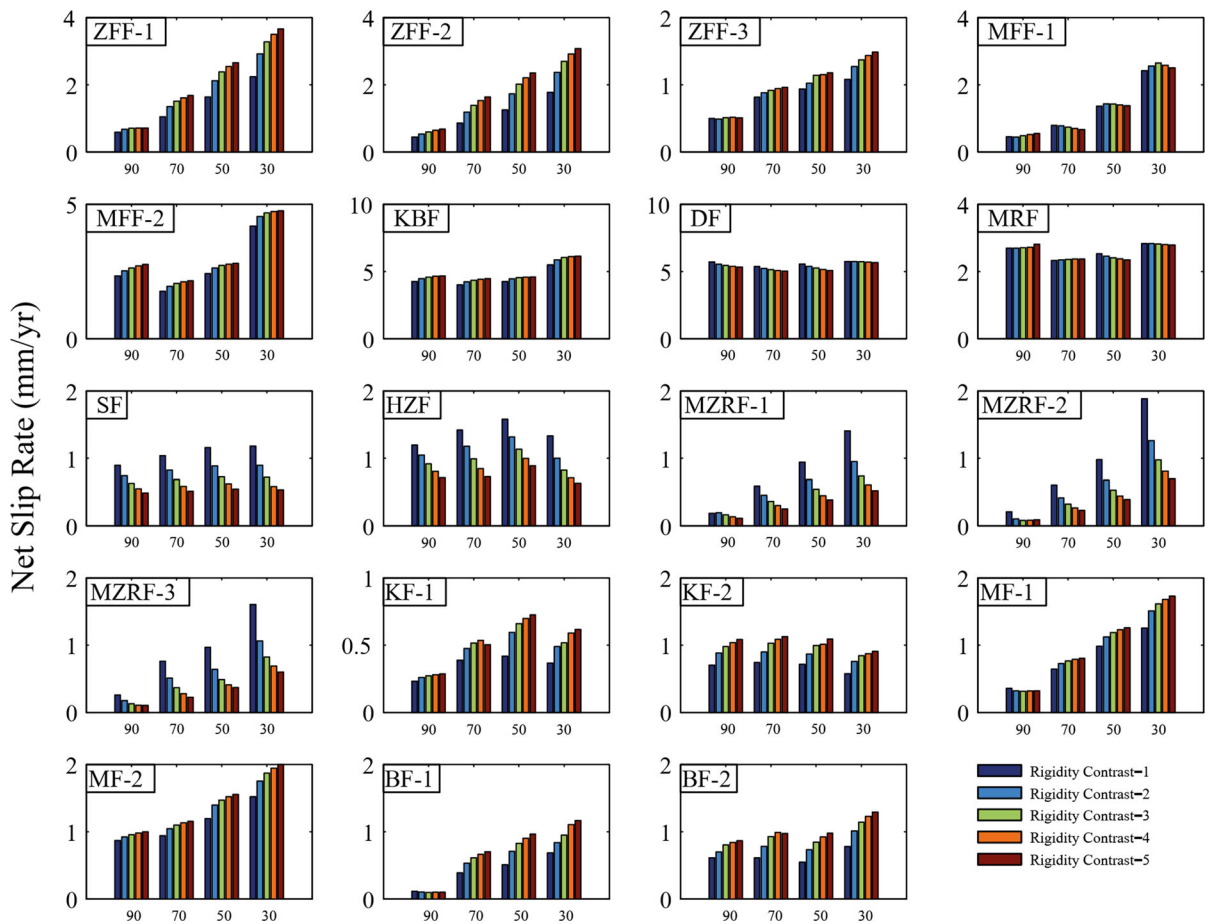


Figure 11
Variation of net slip rates on fault segments due to changes in the dip angle and rigidity contrast

cannot be detected by GPS transect across individual fault. As seen in Table 3, several segments in this region have slip rates of less than ~ 1 mm/year. Determination of accurate slip rates for these segments would be extremely challenging using campaign-mode GPS measurements like those that have already been performed in this region. A network of continuous GPS stations would help to better resolve accurate slip rates for such fault segments in the Zagros.

Table 4 shows the lower and upper limits for the strike-, dip- and net slip rates due to variations in the dip angle and rigidity contrast of the fault system. The maximum variations in the strike-, dip- and net slip rates occur in the Karez Bas (-6 to -4 mm/year), Main Front (seg. 2) (-0.2 to 3.4 mm/year) and

Zagros Front (seg. 1) (0.6 – 3.5 mm/year) faults, respectively. These variations suggest that the lateral heterogeneity and geometric representation of fault systems have dominant roles in estimating the slip budgets of faults in numerical models (BARBA *et al.* 2013; CARAFA and BARBA 2011; COOKE and MARSHALL 2006; MARSHALL *et al.* 2008; MARSHALL and MORRIS 2012).

Previous attempts to estimate the rates of dextral strike-slip motion in the KFS using GPS observations suggest that the Dena, Kazerun, Karez Bas and Main Recent faults slip at rates of 2.9 – 4.5 mm/year, 3 – 4.2 mm/year, 3.1 – 3.7 mm/year and 2.3 – 2.7 mm/year, respectively, and that these slips accommodate most of the differential motion between the North and Central Zagros (TAVAKOLI *et al.* 2008). Considering

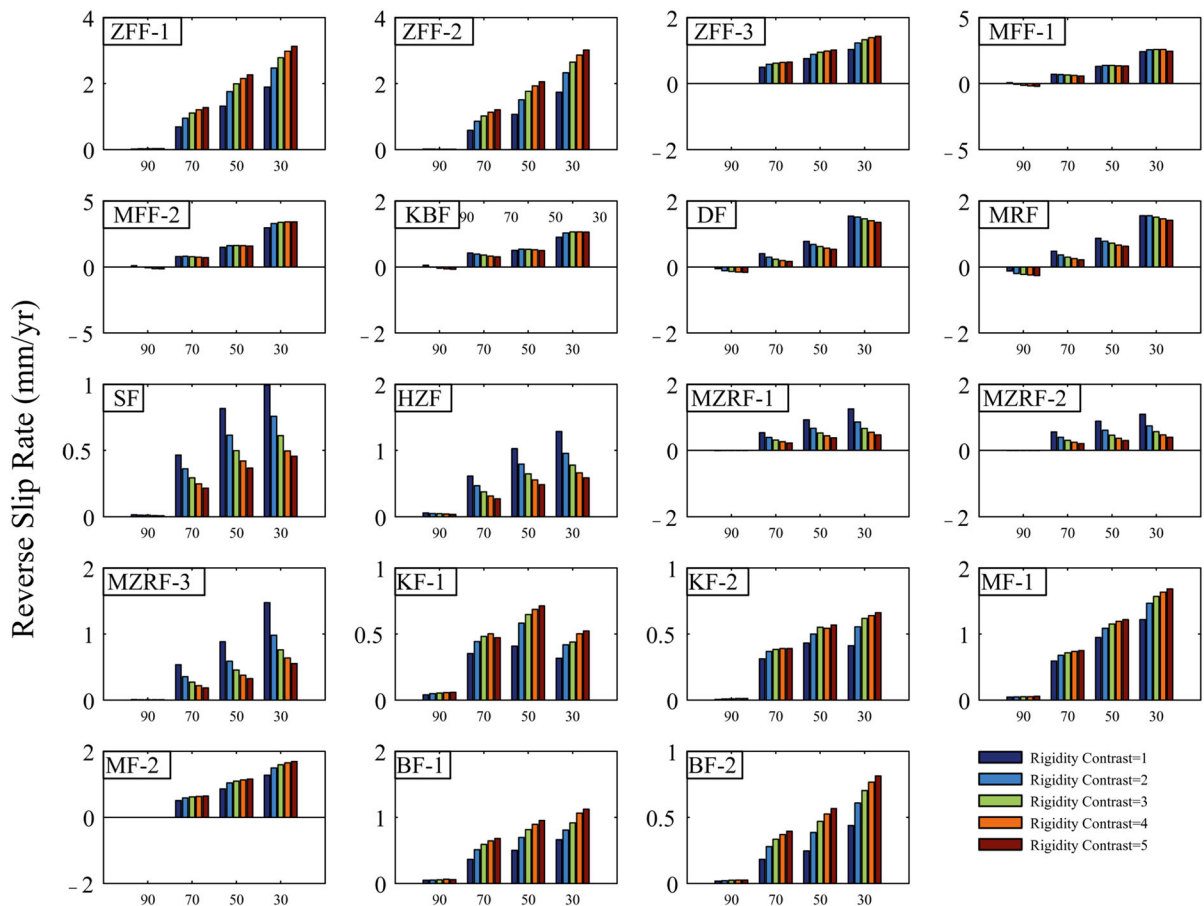


Figure 12
Variation of reverse-slip rates on fault segments due to changes in the dip angle and rigidity contrast

the average dip angle of 50° – 60° , our estimate for the strike-slip rate of the Kazerun segment is 0.7 mm/year . Variations in the rigidity contrast from 1 to 5 and in the dip angle from 30° to 90° affect these values by $\pm 0.4 \text{ mm/year}$ (57%). This estimate is closer to the geological-derived slip rate than to the geodetic slip rate that was derived by TAVAKOLI *et al.* (2008). Our model shows that in addition to the 4 main segments described above, other faults, such as the Zagros Front (seg. 1) (0.9 mm/year), Main Front (seg. 2) (1.9 mm/year), High Zagros (0.9 mm/year) and Mishan (seg. 2) (0.8 mm/year) faults, also accommodate some of the differential motion between the North and Central Zagros (see Table 3).

Of the 19 fault segments that are shown in Fig. 9, the Zagros Front (seg. 1), Zagros Front (seg. 2), Main Front (seg. 1) and Main Front (seg. 2) faults show

reverse slip rates higher than 1 mm/year . All of these segments are located along the southern margin of the region, which indicates the importance of reverse faulting in that area. Orientation of faults with respect to the direction of constraints applied as boundary condition at the boundary of models makes the dip-slip motion more sensitive to a change in dip angle in contrast to the strike-slip motion (Fig. 9). As shown in Fig. 9, the sensitivity is higher for the 4 segments of the Zagros Front (seg. 1 and 2) (0 – 3.1 , 0 – 3 mm/year) and the Main Front (seg. 1 and 2) (-0.2 to 2.6 , -0.2 to 3.4 mm/year) than the other faults. These segments strike approximately perpendicular to the principal contraction orientation, which favors dip-slip motion that can be influenced by changes in the dip angle. Therefore, knowledge of the dip angle is crucial for obtaining a precise estimate of the rate of

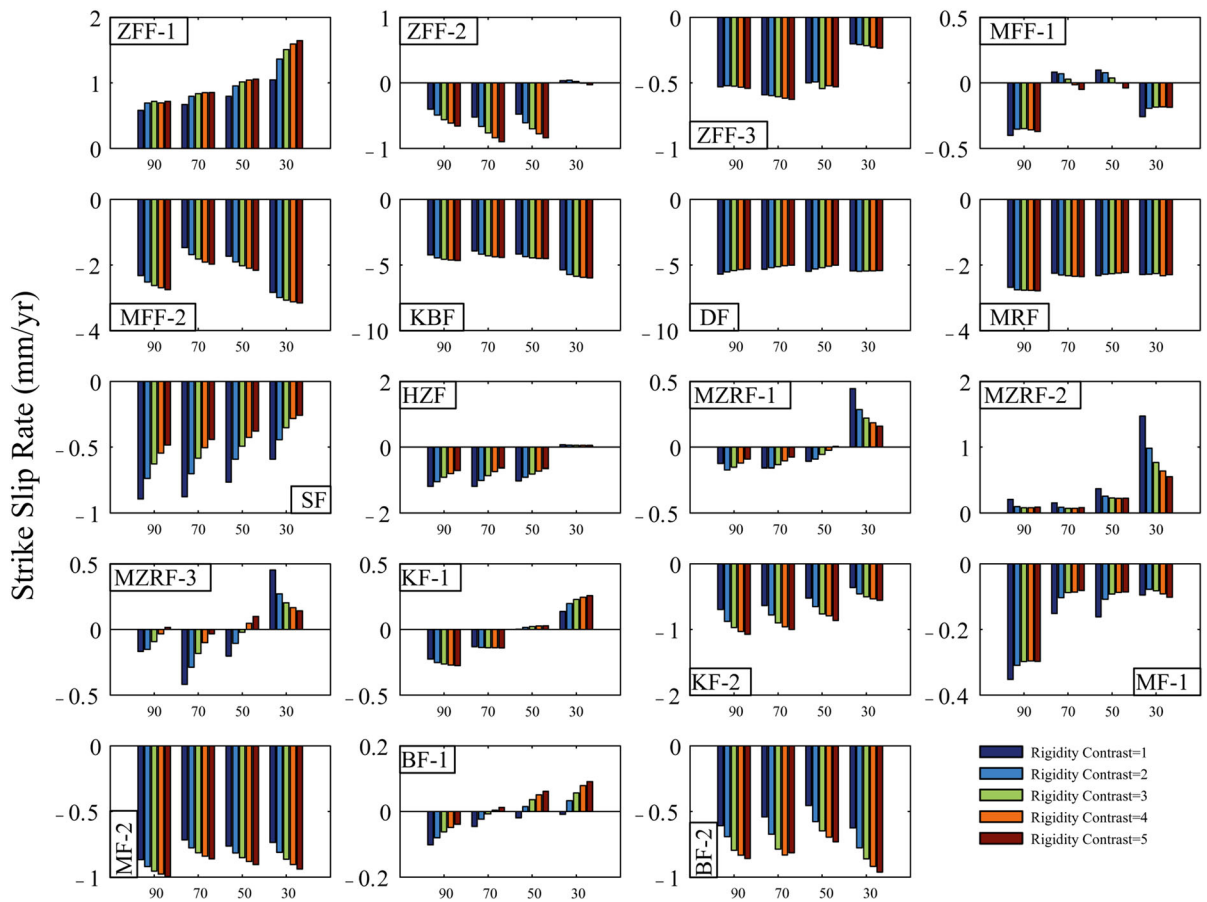


Figure 13
Variation of strike-slip rates on fault segments due to changes in the dip angle and rigidity contrast

reverse slip. This is particularly important for those segments of the KFS that are subject to reverse slip, such as the Zagros Front, Main Front, Kazerun and Mishan faults (Fig. 9). A combination of information from the traces of geologic surfaces, seismicity, seismic reflection profiles, wells and geologic cross sections is, therefore, necessary to derive a precise three-dimensional model of the major faults in the KFS (PLESCH *et al.* 2007).

Of the major faults in the KFS, the Dena and Kazerun faults show good consistency between the contemporary slip rates (Fig. 8; Table 3) and the long-term geologic slip rates (AUTHEMAYOU *et al.* 2009). Our estimate for the Main Recent Fault (2.3 mm/year) is within the range observed by GPS (0.5–4.5 mm/year) but shows a large discrepancy with the long-term geologic slip rates (6–10 mm/

year). Some of this discrepancy may be due to the simple geometry that we used for the modeling. Because of the complexity of several fault strands in this region (AUTHEMAYOU *et al.* 2009), we simplified them using single straight lines in our model. Accommodating the total slip of several fault strands by a single fault trace can result in overestimation of the slip rate. Also, the geological slip is measured on a single fault strand and, therefore, is a lower limit of slip across a fault consisting of several parallel strands. This discrepancy for the Main Recent Fault may be related to model approximations or to the geologic data availability.

Using a 3-D visco-elastic finite element model for the Zagros, the dextral strike-slip rates for the MRF, Dena and Kazerun faults, assuming vertical dips, were 2.3, 4.8 and 2.1 mm/year, respectively (NANKALI

Table 5
Slip rate variation due to change of rigidity contrast

No.	Fault	Rigidity contrast	Strike (mm/year)		Dip (mm/year)		Net (mm/year)		Slip rate variation (%)
			Dip 60°	Dip 50°	Dip 60°	Dip 50°	Dip 60°	Dip 50°	
1	Zagros Front (seg. 1)	1	0.73	0.79	1.00	1.31	1.24	1.54	-23
		2	0.87	0.95	1.35	1.75	1.61	1.99	
2	Zagros Front (seg. 2)	1	-0.50	-0.48	0.82	1.07	0.97	1.17	-28
		2	-0.64	-0.61	1.18	1.51	1.34	1.63	
3	Zagros Front (seg. 3)	1	-0.55	-0.50	0.63	0.76	0.83	0.91	-9
		2	-0.55	-0.49	0.73	0.89	0.91	1.01	
4	Main Front (seg. 1)	1	0.09	0.10	1.00	1.30	1.01	1.31	-2
		2	0.07	0.08	1.03	1.37	1.03	1.37	
5	Main Front (seg. 2)	1	-1.60	-1.74	1.14	1.48	1.97	2.28	-9
		2	-1.80	-1.91	1.20	1.60	2.16	2.49	
6	Kareh Bas	1	-4.06	-4.18	0.46	0.50	4.08	4.21	-5
		2	-4.28	-4.38	0.46	0.54	4.30	4.41	
7	Dena	1	-5.41	-5.49	0.59	0.77	5.45	5.54	3
		2	-5.27	-5.32	0.49	0.68	5.29	5.37	
8	Main Recent	1	-2.29	-2.33	0.67	0.87	2.39	2.48	0.01
		2	-2.30	-2.29	0.57	0.78	2.37	2.42	
9	Sarvestan	1	-0.82	-0.77	0.64	0.82	1.04	1.12	29
		2	-0.65	-0.59	0.49	0.61	0.81	0.85	
10	High Zagros	1	-1.11	-1.02	0.82	1.03	1.38	1.45	20
		2	-0.96	-0.91	0.63	0.79	1.15	1.21	
11	Main Zagros Recent (seg. 1)	1	-0.13	-0.11	0.73	0.92	0.74	0.93	36
		2	-0.13	-0.09	0.53	0.67	0.54	0.67	
12	Main Zagros Recent (seg. 2)	1	0.26	0.37	0.72	0.88	0.77	0.95	45
		2	0.17	0.26	0.50	0.61	0.53	0.66	
13	Main Zagros Recent (seg. 3)	1	-0.31	-0.20	0.71	0.88	0.77	0.90	51
		2	-0.20	-0.11	0.47	0.59	0.51	0.60	
14	Kazerun (seg. 1)	1	-0.07	0.00	0.38	0.41	0.39	0.41	-25
		2	-0.06	0.01	0.51	0.58	0.52	0.58	
15	Kazerun (seg. 2)	1	-0.58	-0.52	0.37	0.43	0.69	0.68	-18
		2	-0.72	-0.65	0.43	0.50	0.84	0.82	
16	Mishan (seg. 1)	1	-0.16	-0.16	0.77	0.95	0.78	0.96	-12
		2	-0.11	-0.11	0.88	1.09	0.89	1.09	
17	Mishan (seg. 2)	1	-0.74	-0.76	0.69	0.86	1.01	1.15	-11
		2	-0.80	-0.82	0.81	1.04	1.14	1.32	
18	Borazjan (seg. 1)	1	-0.03	-0.02	0.43	0.50	0.43	0.50	-28
		2	0.00	0.01	0.60	0.70	0.60	0.70	
19	Borazjan (seg. 2)	1	-0.50	-0.46	0.21	0.25	0.54	0.52	-23
		2	-0.63	-0.58	0.33	0.39	0.71	0.69	

2011). The elastic model (fault system with 90° dips and a rigidity contrast of 2) predicts strike-slip rates for these segments of 2.7, 5.5 and 0.9 mm/year, respectively. The maximum and minimum slip rates in the two models are on the Dena and Kazerun faults. Our estimates for the strike-slip rates of the MRF and the Dena Fault are consistent (discrepancies of less than 15 %) with those obtained by the visco-elastic model, while the Kazerun Fault has a discrepancy of 130 %. Although the assumptions of our model and

the visco-elastic model are different, the slip rates for the two models generally correlate.

Kazerun fault system accommodates different styles of deformation between North and Central Zagros (AUTHEMAYOU *et al.* 2005; BERBERIAN 1995). Using measurements on either side of the Kazerun fault system, WALPERSDORF *et al.* (2006) showed that the accommodation of the convergence differs across the region. Comparing slip rates from finite element models with geology and GPS slip rate (Fig. 8), it

seems that the Dena and Kareh Bas segments are overestimated and the Kazerun segment is underestimated. Part of discrepancy may be related to configuration of the fault system. Previous studies show that fault connectivity and corrugated nonplanar fault surfaces have important role on finite element slip rate and can result in discrepancy between geodetic and geologic slip rates (HERBERT *et al.* 2014; MARSHALL and MORRIS 2012). Also 3D representation of faults in the region that was used in finite element models is based on the approximate upper traces of the fault segments that were fixed by geologic evidence (AUTHEMAYOU *et al.* 2006; BERBERIAN 1995) and is taken to be as the base model.

5. Conclusion

This study presented a 3D finite element model (FEM) to model interseismic deformation of the Kazerun Fault System in the Zagros mountain belt of Iran. The model was used to assess the slip rates and the locking depth for 19 fault segments in the KFS and study the contrast in rigidity between the between the southern and northern areas of the Zagros mountain belt

Our results suggest the existence of a contrast in rigidity between the eastern and western part of the MRF–DF–KBF–MFF faults within the Zagros fold-and-thrust belt, but a constraint on the average dip angle being greater than 30° is required. This constraint is not an artificial constraint, rather a realistic and physical one supported by geological and seismic observations (ALAVI 2007; JACKSON 1980; SEPEHR and COSGROVE 2005; SEPEHR *et al.* 2006; SHERKATI *et al.* 2005; TATAR *et al.* 2004).

Our analysis of the slip budget of 19 fault segments in the KFS provides a more complete and coherent list of strike and dip-slip rates for the fault segments than what has been published previously (TAVAKOLI *et al.* 2008; WALPERSDORF *et al.* 2006). We derived right-lateral motions for the majority of the fault segments in the KFS, which is consistent with the tectonic regime that was derived by inversion of focal mechanisms (ZARIFI *et al.* 2013). The modeling results show that in addition to the 4 main faults (Dena, Kazerun, Kare Bas and Main Recent faults),

which have been studied in detail previously, other faults, such as the Zagros Front, Main Front, High Zagros and Mishan faults, accommodate up to 2.5 mm/year of the differential movement between the North and Central Zagros. The reverse slips on the Zagros Front, Main Front and Mishan segments can reach up to 2 mm/yr and play a significant role in accommodating the differential movement between the North and Central Zagros.

We estimate an average dip-slip rate of 0.7–0.9 mm/yr (average of all fault segments), which is consistent with geological estimates of the uplift rate (FALCON 1974). The good match between the slip rates obtained from the model with those obtained by previous geological and geodetic studies suggests that the model is representative of the geometric and physical properties of Kazerun Fault System. Furthermore, because the deformation in our model is driven by the contemporary GPS velocity vectors, the results show that the present-day strike- and dip-slip rates in the Kazerun Fault System are generally compatible with the long time geological deformation.

Active fault zones in Iran (Zagros, Alborz, Kopeh-Dagh, Makran, northwestern and eastern Iran) provide a potentiality to use numerical modeling to investigate detailed fault kinematics and rates in these complex regions. Using the FEM, we are able to derive off-fault motions for all active segments in the region that cannot be detected by GPS transect across individual fault segment. The numerical modeling indicates that the fault geometry in the model has an important role in determining the accurate slip budget. Having a set of validated geological and geodetic slip rates for a number of fault segments and comparing them with finite element-derived slip rates help evaluate the effect of a lot of physical parameters such as layering, frictional or non-frictional basal decollement, fault friction, fault connectivity and nonplanar fault surface on the derived slip rates.

Acknowledgments

The manuscript has largely been benefitted by constructive and critical comments of the associate editor, Salvatore Barba, and two anonymous reviewers.

REFERENCES

- ALAVI, M., 2007. *Structures of the Zagros fold-thrust belt in Iran*. American Journal of science 307, 1064–1095.
- ALLMENDINGER, R.W., REILINGER, R., LOVELESS, J., 2007. *Strain and rotation rate from GPS in Tibet, Anatolia, and the Altiplano*. Tectonics 26.
- ALTAMIMI, Z., SILLARD, P., BOUCHER, C., 2002. *ITRF2000: A new release of the International Terrestrial Reference Frame for earth science applications*. Journal of Geophysical Research: Solid Earth (1978–2012) 107, ETG 2-1–ETG 2-19.
- AMORUSO, A., BARBA, S., CRESCENTINI, L., MEGNA, A., 2013. *Inversion of synthetic geodetic data for dip-slip faults: clues to the effects of lateral heterogeneities and data distribution in geological environments typical of the Apennines (Italy)*. Geophysical Journal International 192, 745–758.
- AUTHEMAYOU, C., BELLIER, O., CHARDON, D., BENEDETTI, L., MALEKZADE, Z., CLAUDE, C., ANGELETTI, B., SHABANIAN, E., ABBASSI, M.R., 2009. *Quaternary slip-rates of the Kazerun and the Main Recent Faults: Active strike-slip partitioning in the Zagros fold-and-thrust belt*. Geophysical Journal International 178, 524–540.
- AUTHEMAYOU, C., BELLIER, O., CHARDON, D., MALEKZADE, Z., ABBASSI, M., 2005. *Role of the Kazerun fault system in active deformation of the Zagros fold-and-thrust belt (Iran)*. Comptes Rendus Geoscience 337, 539–545.
- AUTHEMAYOU, C., CHARDON, D., BELLIER, O., MALEKZADEH, Z., SHABANIAN, E., ABBASSI, M.R., 2006. *Late Cenozoic partitioning of oblique plate convergence in the Zagros fold-and-thrust belt (Iran)*. Tectonics 25.
- BARBA, S., FINOCCHIO, D., SIKDAR, E., BURRATO, P., 2013. *Modelling the interseismic deformation of a thrust system: seismogenic potential of the Southern Alps*. Terra Nova 25, 221–227.
- BERBERIAN, M., 1995. *Master “blind” thrust faults hidden under the Zagros folds: active basement tectonics and surface morpho-tectonics*. Tectonophysics 241, 193–224.
- CARAFI, M., BARBA, S., 2011. *Determining rheology from deformation data: The case of central Italy*. Tectonics 30.
- CARBON, D., 1996. *Tectonique post-obduction des montagnes d’Oman dans le cadre de la convergence Arabie-Iran*. Evénements sismiques d’âge pléistocène en France: ruptures de surface et quantification de la déformation.
- COOKE, M.L., MARSHALL, S.T., 2006. *Fault slip rates from three-dimensional models of the Los Angeles metropolitan area, California*. Geophysical research letters 33, L21313.
- FALCON, N., 1967. *The geology of the north-east margin of the Arabian basement shield*. Advancement Science 24, 1–12.
- FALCON, N.L., 1969. *Problems of the relationship between surface structure and deep displacements illustrated by the Zagros Range*. Geological Society, London, Special Publications 3, 9–21.
- FALCON, N.L., 1974. *Southern Iran: Zagros Mountains*. Geological Society, London, Special Publications 4, 199–211.
- GRIFFITH, W.A., COOKE, M.L., 2005. *How Sensitive Are Fault-Slip Rates in the Los Angeles Basin to Tectonic Boundary Conditions?* Bulletin of the Seismological Society of America 95, 1263–1275.
- HAGER, B.H., LYZENGA, G.A., DONNELLAN, A., DONG, D., 1999. *Reconciling rapid strain accumulation with deep seismogenic fault planes in the Ventura basin, California*. Journal of Geophysical Research: Solid Earth (1978–2012) 104, 25207–25219.
- HERBERT, J.W., COOKE, M.L., MARSHALL, S.T., 2014. *Influence of fault connectivity on slip rates in southern California: Potential impact on discrepancies between geodetic derived and geologic slip rates*. Journal of Geophysical Research: Solid Earth 119, 2342–2361.
- HSU, Y.J., SIMONS, M., WILLIAMS, C., CASAROTTI, E., 2011. *Three-dimensional FEM derived elastic Green’s functions for the coseismic deformation of the 2005 Mw 8.7 Nias-Simeulue, Sumatra earthquake*. Geochemistry, Geophysics, Geosystems 12.
- HUGHES, K.L., MASTERLARK, T., MOONEY, W.D., 2011. *Pore-fluid migration and the timing of the 2005 M8. 7 Nias earthquake*. Lithosphere 3, 170–172.
- JACKSON, J., 1980. *Reactivation of basement faults and crustal shortening in orogenic belts*.
- JACKSON, J., FITCH, T., 1981. *Basement faulting and the focal depths of the larger earthquakes in the Zagros mountains (Iran)*. Geophysical Journal International 64, 561–586.
- LOHMAN, R.B., SIMONS, M., 2005. *Locations of selected small earthquakes in the Zagros mountains*. Geochemistry, Geophysics, Geosystems 6.
- MAGGI, A., JACKSON, J., PRIESTLEY, K., BAKER, C., 2000. *A re-assessment of focal depth distributions in southern Iran, the Tien Shan and northern India: do earthquakes really occur in the continental mantle?* Geophysical Journal International 143, 629–661.
- MANAMAN, N.S., SHOMALI, H., 2010. *Upper mantle S-velocity structure and Moho depth variations across Zagros belt, Arabian–Eurasian plate boundary*. Physics of the Earth and Planetary Interiors 180, 92–103.
- MARSHALL, S.T., COOKE, M.L., OWEN, S.E., 2008. *Effects of non-planar fault topology and mechanical interaction on fault-slip distributions in the Ventura Basin, California*. Bulletin of the Seismological Society of America 98, 1113–1127.
- MARSHALL, S.T., COOKE, M.L., OWEN, S.E., 2009. *Interseismic deformation associated with three-dimensional faults in the greater Los Angeles region, California*. Journal of Geophysical Research: Solid Earth (1978–2012) 114.
- MARSHALL, S.T., FUNNING, G.J., OWEN, S.E., 2013. *Fault slip rates and interseismic deformation in the western Transverse Ranges, California*. Journal of Geophysical Research: Solid Earth 118, 4511–4534.
- MARSHALL, S.T., MORRIS, A.C., 2012. *Mechanics, slip behavior, and seismic potential of corrugated dip-slip faults*. Journal of Geophysical Research: Solid Earth (1978–2012) 117.
- MASTERLARK, T., 2003. *Finite element model predictions of static deformation from dislocation sources in a subduction zone: Sensitivities to homogeneous, isotropic, Poisson-solid, and half-space assumptions*. Journal of Geophysical Research 108, 2540.
- MASTERLARK, T., DEMETS, C., WANG, H., SANCHEZ, O., STOCK, J., 2001. *Homogeneous vs heterogeneous subduction zone models: Coseismic and postseismic deformation*. Geophysical research letters 28, 4047–4050.
- MASTERLARK, T., HANEY, M., DICKINSON, H., FOURNIER, T., SEARCY, C., 2010. *Rheologic and structural controls on the deformation of Okmok volcano, Alaska: FEMs, InSAR, and ambient noise tomography*. Journal of Geophysical Research: Solid Earth (1978–2012) 115.
- MASTERLARK, T., WANG, H.F., 2002. *Transient stress-coupling between the 1992 Landers and 1999 Hector Mine, California, earthquakes*. Bulletin of the Seismological Society of America 92, 1470–1486.

- NANKALI, H., 2011. *Slip rate of the Kazerun Fault and Main Recent Fault (Zagros, Iran) from 3D mechanical modeling*. Journal of Asian Earth Sciences 41, 89–98.
- NI, J., BARAZANGI, M., 1986. *Seismotectonics of the Zagros continental collision zone and a comparison with the Himalayas*. Journal of Geophysical Research: Solid Earth (1978–2012) 91, 8205–8218.
- NILFOROUSHAN, F., MASSON, F., VERNANT, P., VIGNY, C., MARTINOD, J., ABBASSI, M., NANKALI, H., HATZFELD, D., BAYER, R., TAVAKOLI, F., 2003. *GPS network monitors the Arabia-Eurasia collision deformation in Iran*. Journal of Geodesy 77, 411–422.
- PAUL, A., KAVIANI, A., HATZFELD, D., VERGNE, J., MOKHTARI, M., 2006. *Seismological evidence for crustal-scale thrusting in the Zagros mountain belt (Iran)*. Geophysical Journal International 166, 227–237.
- PLESCH, A., SHAW, J.H., BENSON, C., BRYANT, W.A., CARENA, S., COOKE, M., DOLAN, J., FUIS, G., GATH, E., GRANT, L., 2007. *Community fault model (CFM) for southern California*. Bulletin of the Seismological Society of America 97, 1793–1802.
- SAVAGE, J., 1983. *A dislocation model of strain accumulation and release at a subduction zone*. Journal of Geophysical Research: Solid Earth (1978–2012) 88, 4984–4996.
- SAVAGE, J., PRESCOTT, W., 1978. *Asthenosphere readjustment and the earthquake cycle*. Journal of Geophysical Research: Solid Earth (1978–2012) 83, 3369–3376.
- SCOTT, W.R., 1981. *Rational, natural, and open systems*. Englewood Cliffs, NJ: Prentice Hall.
- SEPEHR, M., COSGROVE, J., 2005. *Role of the Kazerun Fault Zone in the formation and deformation of the Zagros Fold-Thrust Belt, Iran*. Tectonics 24.
- SEPEHR, M., COSGROVE, J., MOIENI, M., 2006. *The impact of cover rock rheology on the style of folding in the Zagros fold-thrust belt*. Tectonophysics 427, 265–281.
- SHERKATI, S., MOLINARO, M., FRIZON DE LAMOTTE, D., LETOUZEY, J., 2005. *Detachment folding in the Central and Eastern Zagros fold-belt (Iran): salt mobility, multiple detachments and late basement control*. Journal of Structural Geology 27, 1680–1696.
- TALEBIAN, M., JACKSON, J., 2004. *A reappraisal of earthquake focal mechanisms and active shortening in the Zagros mountains of Iran*. Geophysical Journal International 156, 506–526.
- TATAR, M., HATZFELD, D., GHAFORY-ASHTIANY, M., 2004. *Tectonics of the Central Zagros (Iran) deduced from microearthquake seismicity*. Geophysical Journal International 156, 255–266.
- TATAR, M., HATZFELD, D., MARTINOD, J., WALPERSDORF, A., GHAFORY-ASHTIANY, M., CHÉRY, J., 2002. *The present-day deformation of the central Zagros from GPS measurements*. Geophysical research letters 29, 33-1 to 33-4. doi:10.1029/2002GL015159.
- TAVAKOLI, F., WALPERSDORF, A., AUTHEMAYOU, C., NANKALI, H., HATZFELD, D., TATAR, M., DJAMOUR, Y., NILFOROUSHAN, F., COTTE, N., 2008. *Distribution of the right-lateral strike-slip motion from the Main Recent Fault to the Kazerun Fault System (Zagros, Iran): Evidence from present-day GPS velocities*. Earth and Planetary Science Letters 275, 342–347.
- VERNANT, P., CHÉRY, J., 2006. *Mechanical modelling of oblique convergence in the Zagros, Iran*. Geophysical Journal International 165, 991–1002.
- VERNANT, P., NILFOROUSHAN, F., HATZFELD, D., ABBASSI, M., VIGNY, C., MASSON, F., NANKALI, H., MARTINOD, J., ASHTIANY, A., BAYER, R., 2004. *Present-day crustal deformation and plate kinematics in the Middle East constrained by GPS measurements in Iran and northern Oman*. Geophysical Journal International 157, 381–398.
- WALPERSDORF, A., HATZFELD, D., NANKALI, H., TAVAKOLI, F., NILFOROUSHAN, F., TATAR, M., VERNANT, P., CHÉRY, J., MASSON, F., 2006. *Difference in the GPS deformation pattern of North and Central Zagros (Iran)*. Geophysical Journal International 167, 1077–1088.
- ZARIFI, Z., NILFOUROUSHAN, F., RAEESI, M., 2013. *Crustal stress Map of Iran: Insight from seismic and geodetic computations*. Pure and Applied Geophysics, 1–18.

(Received November 13, 2013, revised January 31, 2015, accepted March 12, 2015, Published online April 1, 2015)